Topological Correlations in Colloidal Aggregation

J.C. Earnshaw and D.J. Robinson
The Department of Pure and Applied Physics, The Queen's University of Belfast, Belfast BT7 1NN, Northern Ireland
(Received 28 January 1994)

Topological properties of cluster-cluster aggregation in two dimensions have been studied. In the diffusion-limited case these properties indicate that the system, apart from a scale change as the clusters grow, is in a stationary state and resembles an ideal random cellular network. For the reaction-limited case the system is nonstationary and is governed by specific physical forces.

PACS numbers: 64.60.Cn, 05.40.+j, 64.75.+g, 82.70.Dd

Recent interest in colloidal aggregation has largely been driven by the concepts of fractal geometry. However, very recently, intercluster correlations have been found for diffusion-limited cluster-cluster aggregation (DLCA). These arise from interactions between the growing clusters, via mutually exclusive depletion zones within which essentially all monomers have been mopped up. In sufficiently dense colloidal systems DLCA leads to a stationary scaling state: both the structure function $S(q,t)$ and the distribution of intercluster separation $P(x)$ scale to universal functions. These effects have been observed for both two- [1] and three-dimensional [2] systems, but are not evident for the reaction-limited case (RLCA). The depletion zones for DLCA can be considered to partition the system into a network of cells. In such networks, the natural focus is on topological, rather than metric properties. In this paper we approach cluster-cluster aggregation in this way, considering various topological functions. We follow studies of cell networks, such as soap froths [3].

Many cellular networks, of diverse origins, appear indistinguishable: specific physical forces are irrelevant. Statistical equilibrium derives from maximizing the entropy of the structure subject to the relevant constraints [4]. Here the constraints of topology and normalization of probability lead to intercell topological correlations. Adding the requirement of space filling yields Lewis's law [5], the equation of state of an ideal random system, relating the average size and shape of cells. Departures from this law indicate the relevance of specific physical forces.

Our experimental methods have been described elsewhere [6(a)]. In brief, polystyrene latex spheres of ~ 1 μm diameter were spread on the surface of an aqueous subphase. Area fractions (ϕ) were rather high, typically $\approx 10\%$. The particles are highly charged and interact via long-range forces [7]. Adding salt ($CaCl_2$) to the subphase induced irreversible aggregation, which proceeded to gelation over a period of hours. Images grabbed at various times (measured from initiation of aggregation) represent quasirandomly selected samples due to some mobility of the colloidal monolayers [6(a)].

The structures observed for salt concentrations $\gtrsim 0.5M$ were consistent with DLCA (Fig. 1), and at lower concentrations with RLCA (Fig. 2) [6(a)]. In all cases there was a crossover from slow to rapid growth kinetics (Fig. 3) [6(b)]; DLCA appears at high concentrations only after this crossover [6(c)]. It was in this rapid, DLCA regime that scaling of $S(q,t)$ and $P(x)$ was observed [1]. We therefore restrict the present considerations to this regime ($t \geq 60$ min) and the similar rapid growth phase for RLCA ($t \geq 225$ min). We present data for two typical experiments, for $0.23M$ and $0.73M$, the metric properties of which have been considered elsewhere [1].

We consider the Voronoi construction [8] based on the centers of gravity of all clusters wholly contained within an image (Figs. 1 and 2); other clusters have indeterminate centers of gravity. The analysis becomes impractical when clusters spanning the image appear, limiting this study to $t \leq 105$ min (DLCA) and ≤ 315 min (RLCA).

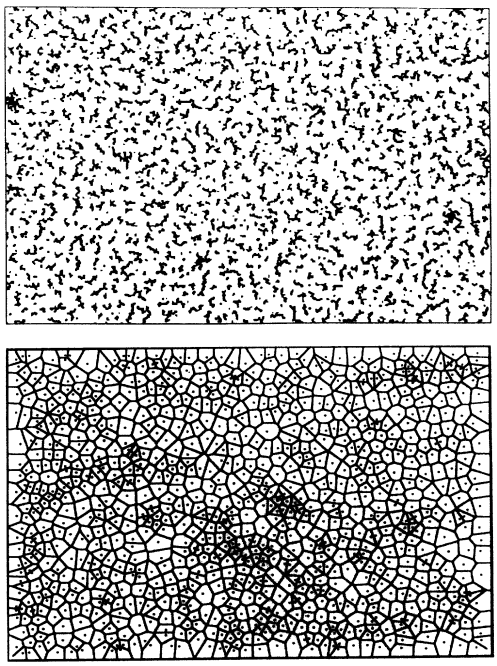

FIG. 1. Binarized video image (730×486 μm^2) of the colloidal monolayer on the $0.73M$ subphase at 75 min (1005 clusters), and the corresponding Voronoi diagram (see text).

0031-9007/94/72(23)/3682(4)$06.00

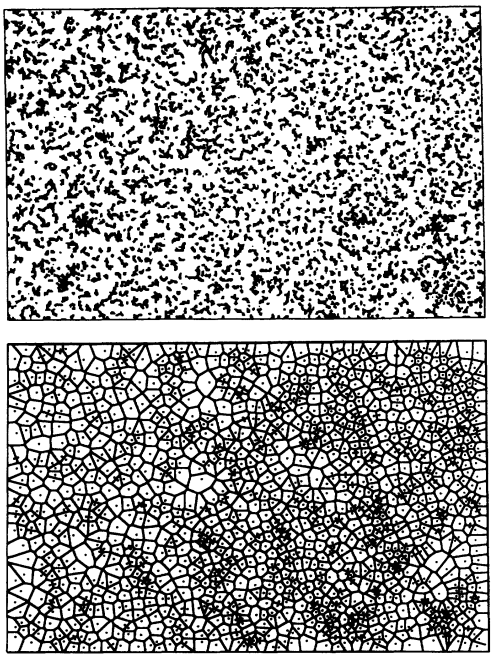

FIG. 2. As in Fig. 1, but for $0.23M$ at 285 min (1339 clusters). The Voronoi diagram is noticeably less homogeneous in this case.

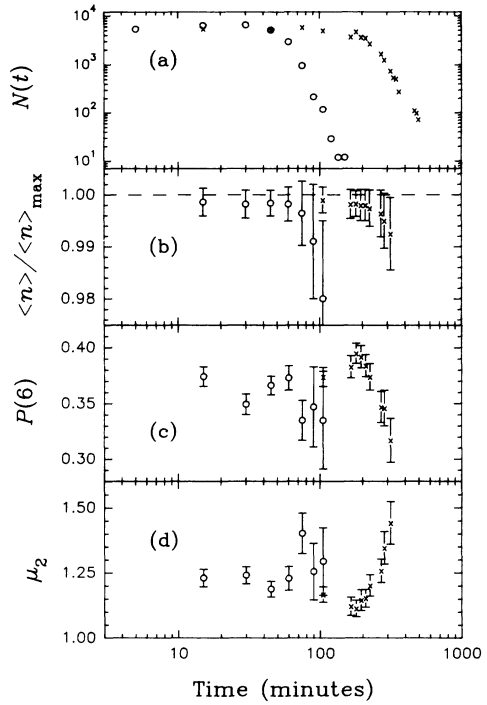

FIG. 3. The variation with time of various quantities for aggregation on a $0.23M$ $CaCl_2$ subphase (×) and for $0.73M$ (○). (a) Number of clusters in micrograph; note the crossover from slow to rapid growth. (b) Average number of sides of a cell, compared to the maximum value of $\langle n \rangle$ for N points in a plane. (c) Fraction of cells having six sides. (d) Second central moment of $P(n)$.

The Voronoi diagrams comprise close-packed arrays of irregular polygons (cells), each delimiting the neighborhood of a given point.

$P(n)$, the distribution of the number of edges of the cells (coordination number), is not very informative in itself, so we discuss its moments and other characteristics (Fig. 3). For an infinite array of points in a plane, Euler's theorem gives $\langle n \rangle = 6$; for N points $\langle n \rangle \leq 6 - 12/N$ [8]. We thus compare the observed $\langle n \rangle$ with this upper limit, $\langle n \rangle_{\max}$. As aggregation proceeds $\langle n \rangle / \langle n \rangle_{\max}$ falls somewhat, but remains consistent with unity. DLCA and RLCA are not readily distinguishable. However, $P(6)$ and the second central moment, μ_2 $[\equiv \sum_n (n - \langle n \rangle)^2 P(n)]$, differ for the two cases. [Higher moments of $P(n)$ are less well defined.] For RLCA these statistics evolve with time, $P(6)$ falling as μ_2 rises. Both indicate an increasing degree of inhomogeneity in RLCA, visible in the micrographs as small clusters persist into late stages of aggregation [1]. In contrast, for DLCA ($t \geq 60$ min) both $P(6)$ and μ_2 appear to remain constant within errors as aggregation proceeds. Thus, as well as the metric properties mentioned above, $P(n)$ is stationary for a colloidal monolayer undergoing DLCA.

We now turn to various topological correlations. The number of sides of adjoining cells are correlated: many-sided cells have few-sided neighbors and vice versa. A widely obeyed semiempirical formula, the Aboav-Weaire law [4,9], states that the mean number of sides of cells adjoining an n-sided cell is

$$m(n) = 6 - a + (6a + \mu_2)/n, \qquad (1)$$

where the parameter a is generally ~ 1. The Aboav-Weaire law comprises three statements: (i) $m(n)$ is linear in $1/n$, (ii) $a \sim 1$, so that the gradient is about 7, (iii) $m(6) = \langle n \rangle + \mu_2/6$. The last is a special case of a rigorous sum rule due to Weaire [10]: $\langle nm(n) \rangle = \langle n \rangle^2 + \mu_2$. For finite networks $\langle n \rangle \neq 6$ and the law becomes [11]

$$m(n) = \langle n \rangle - a + [\langle nm(n) \rangle - \langle n \rangle^2 + \langle n \rangle a]/n. \qquad (2)$$

The common practice of plotting $nm(n)$ versus n can conceal deviations from the law as $m(n)$ does not vary much with n. It is preferable to plot $m(n)$ versus $1/n$.

Finite system effects caused $m(n)$ to depart significantly from this law when $n \geq 9$. Such many-sided cells tended to be associated with each other in the periphery of the Voronoi diagram. The computation was thus restricted to "inner" n-sided cells (defined as those not extending beyond the video image).

For DLCA the data for the inner cells essentially superimpose and are entirely consistent with linear dependance upon $1/n$ (Fig. 4), the average slope and intercept being 7.28 ± 0.21 and 4.907 ± 0.037, respectively. $m(6)$ agrees with $\langle n \rangle + \mu_2/6$. With Eq. (2), and using the average μ_2 and $\langle n \rangle$ from the appropriate times (Fig. 3), the slope and intercept yield consistent values of a: 0.997 ± 0.036 and 0.994 ± 0.050. DLCA thus ac-

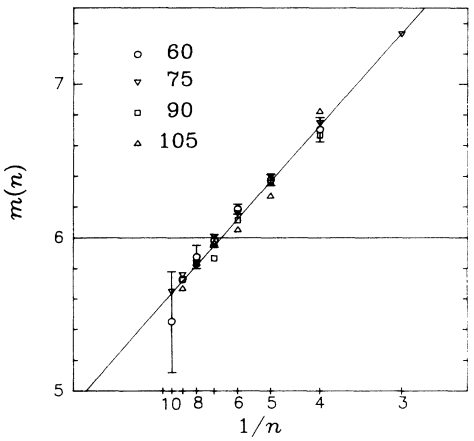

FIG. 4. Mean number of sides of cells surrounding an n-sided cell for DLCA (times as legend). Errors are only shown for the 60 min data; other errors are larger. The line is the weighted average of the several best-fit linear variations.

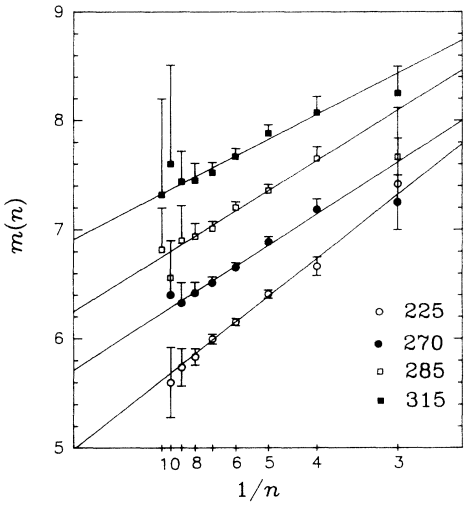

FIG. 5. As for Fig. 4, but for RLCA. For clarity, data for later times are vertically displaced and only half error bars shown. Linear fits are shown.

cords well with the Aboav-Weaire law in all its aspects. Weaire's rigorous sum rule is obeyed for *all* n-sided cells.

For RLCA, $m(n)$ at different times do not collapse to a common variation with $1/n$ (Fig. 5). While $m(n) \propto 1/n$, and $m(6) = \langle n \rangle + \mu_2/6$, a was not constant. Linear fits to the data evolved with time, reflecting a systematic decrease of a. Thus, while the Aboav-Weaire law seems valid, these data again show that a colloidal system undergoing RLCA is nonstationary. The inhomogeneity characteristic of RLCA leads to larger uncertainties on the various correlations, making it more difficult to ascertain their agreement with theory.

A further two-cell correlation function [12], $M_l(n)$, is the average number of l-sided cells adjoining an n-sided one, usually considered scaled by $P(l)$:

$$A_{ln} = M_l(n)/P(l) = M_n(l)/P(n) = A_{nl}. \quad (3)$$

If A_{ln} is linear in n then the Aboav-Weaire law follows from maximum entropy. Linearity of A_{ln} in l and n entails the unique relation [13]

$$A_{ln} = n + l - 6 - a/\mu_2(n-6)(l-6). \quad (4)$$

The data for inner n-sided cells in the present cases seem to be consistent with this, within rather large errors. It is easier to present the data scaled to a universal function of n. By comparing P_{ln}, the probability that cells with l and n sides are neighbors, with the similar probability for an ideal, correlation-free arrangement of cells, a topological short-range order coefficient can be defined [11]

$$\beta_{ln} = 6A_{ln}/ln - 1. \quad (5)$$

Evidently, for A_{ln} linear in l and n [Eq. (4)], the scaled form

$$\gamma_{ln} = \beta_{ln}/(1 - 6/l) \quad (l \neq 6) \quad (6)$$

must be a universal function of $6/n - 1$. We take $\langle n \rangle = 6$, in view of the errors on A_{ln}.

Figure 6 shows the γ_{ln} for DLCA at 60 min (statistics worse for later times). The data are consistent with the expected universal function derived from linearity of A_{ln}, using a and μ_2 from Fig. 3. Within the larger errors γ_{ln} for RLCA is also consistent with this relation. For both cases β_{ln} is zero for l or $n = 6$: as expected, six-sided cells are uncorrelated with their neighbors.

Lewis's law [5] relates the average area of cells to the number of sides: $\langle A(n) \rangle \propto n$. Figure 7 shows that $\langle A(n) \rangle$ for DLCA for inner cells is linearly proportional to n. We thus recover Lewis's law, which is the equation of state for ideal random cellular networks [4].

We can conclude that, as regards intercluster structure, in DLCA the system achieves a state which is stationary with respect to both geometrical [1] and topological prop-

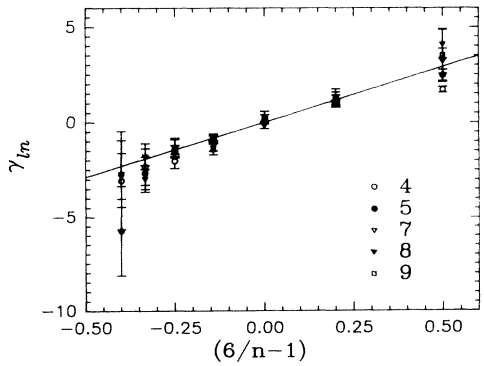

FIG. 6. Normalized topological short-range order coefficients for DLCA at 60 min (l as legend). The data are in accord with the line, representing the unique linear relation, $\gamma_{ln} = -(1 + 6a/\mu_2)(6/n - 1)$.

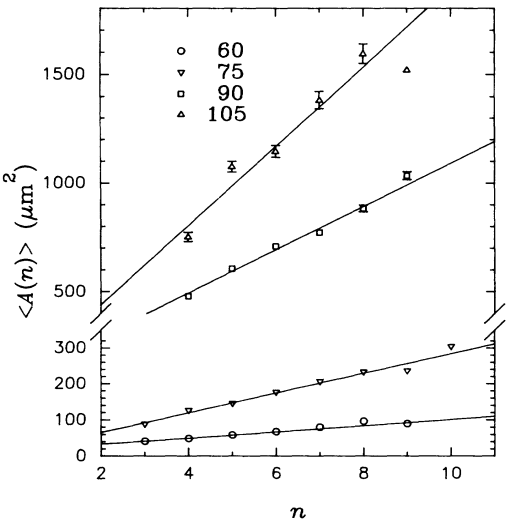

FIG. 7. Average area of n-sided Voronoi polygons for DLCA (times as legend), showing accord with Lewis's law. The point for $n = 9$, $t = 105$ min derives from a single cell.

erties, apart from the change of scale inherent in aggregation. The correlations explored here, A_{ln} and Lewis's law, are consistent with maximum entropy [4]. In particular, the applicability of Lewis's law implies that DLCA corresponds to statistical equilibrium. Lewis's law derives from purely mathematical constraints [4]: physical forces play no role in such a structure.

RLCA differs, neither geometrical nor topological properties being stationary. $\langle A(n) \rangle$ appears quadratically, rather than linearly, related to n. The mean perimeter of an n-sided cell is more nearly proportional to n. The implications are not entirely clear, but it resembles the case of metallurgical grains, for which growth is driven by the energy stored in the grain boundaries [4]. It may be that similar arguments apply for RLCA: cells grow as clusters grow, energy being required to overcome the electrostatic repulsion of the incompletely screened colloidal particles. At all events RLCA is not governed by the equation of state of an ideal cellular network; the departures from Lewis's law demonstrate that the cellular structure is determined by particular, probably local, physical interactions.

This work has been supported by the SERC.

[1] D.J. Robinson and J.C. Earnshaw, Phys. Rev. Lett. **71**, 715 (1993).
[2] M. Carpineti and M. Giglio, Phys. Rev. Lett. **68**, 3327 (1992).
[3] C.S. Smith, Sci. Am. **190**, 58 (1954); D. Weaire and N. Rivier, Contemp. Phys. **25**, 59 (1984).
[4] N. Rivier, Philos. Mag. B **52**, 795 (1985); Physica (Amsterdam) **23D**, 129 (1986).
[5] F.T. Lewis, Anat. Record **38**, 341 (1928).
[6] (a) D.J. Robinson and J.C. Earnshaw, Phys. Rev. A **46**, 2045 (1992); (b) **46**, 2055 (1992); (c) **46**, 2065 (1992).
[7] A.J. Hurd, J. Phys. A **18**, L1055 (1985).
[8] F.P. Preparata and M.I. Shamos, *Computational Geometry* (Springer-Verlag, New York, 1985), Chap. 4.
[9] D.A. Aboav, Metallography **3**, 383 (1970); D. Weaire, *ibid.* **7**, 157 (1974).
[10] C.J. Lambert and D. Weaire, Philos. Mag. B **47**, 445 (1983).
[11] G. Le Caër and R. Delannay, J. Phys. A **26**, 3931 (1993).
[12] M.A. Peshkin, K.J. Strandburg, and N. Rivier, Phys. Rev. Lett. **67**, 1803 (1991).
[13] R. Delannay, G. Le Caër, and M. Khatun, J. Phys. A **25**, 6193 (1992).